Quantum theory of optical pulse propagation through an absorbing and dispersive slab

M. Artoni[1,2] and R. Loudon[1]
[1]*Department of Physics, University of Essex, Colchester CO4 3SQ, England*
[2]*Department of Physics and Applied Physics, University of Strathclyde, Glasgow G4 0NG, Scotland*
(Received 14 August 1996)

We apply a recently developed scheme for electromagnetic field quantization in dispersive and absorbing dielectrics to calculate the effects of perpendicular propagation through a finite-temperature dielectric slab on the properties of an incident pulse of light. The theory applies to incident pulses of nonclassical light and also reproduces the results for classical pulses in the appropriate limit. The transmitted pulse is assumed to be measured by a detector that receives radiation only from the direction normal to the slab surfaces. The Poynting vector of the transmitted light includes contributions from the incident pulse, whose shift in peak position and additional broadening or narrowing are determined, and from the thermal emission of the slab, which tends to a black-body form in the appropriate limits. [S1050-2947(97)02601-2]

PACS number(s): 42.50.−p

I. INTRODUCTION

The electromagnetic field has recently been quantized for several sample geometries of a dispersive and absorbing dielectric material [1,2] following earlier work that is extensively reviewed in these references. The results cover the formal quantization procedures and the forms of the electromagnetic field operators for wave propagation perpendicular to the sample surfaces. The purpose of the present paper is to apply this formalism to the transmission of an optical pulse through a dielectric slab that is maintained at a finite temperature. It is assumed that the transmitted pulse is viewed by a photodetector whose field of view is restricted to the direction perpendicular to the slab surfaces, so that the field variations occur in one dimension only.

The various optical properties of the incident pulse are modified by the dispersion and absorption in the dielectric and by the reflections from the slab surfaces. Some of these modifications result in distortions of the transmitted pulse in comparison with the properties of the incident pulse. The effects of propagation through an infinite dispersive and absorbing medium on a Gaussian light pulse were treated by Garrett and McCumber [3] and some of the predicted effects were confirmed in experiments by Chu and Wong [4] on layers of GaP:N. In particular, these papers established the importance of the group velocity, calculated from the real part of the refractive index, in determining the propagation of the pulse envelope. The original theory for an unbounded medium [3] has been extended by Halevi and co-workers [5–9] and more recently by Japha and Kurizki [10], to include the effects of multiple reflections at the sample surfaces: these effects are important in the interpretation [10,11] of the observed phenomenon of apparent superluminal pulse propagation through multilayer dielectric barriers [12,13].

In addition to these distortion effects, at elevated temperatures, the features of the transmitted pulse are obscured by the presence of thermal emission from the slab. Both these contributions to the emission are treated in the present paper, and the results extend previous theoretical work on pulse propagation into the quantum domain. We shall show that the same pulse distortions are predicted by the quantum and classical theories. However, for incident light of a nonclassical nature, there are also modifications of the quantum coherence and correlation properties of the pulse that can only be described by a quantum theory, and these will be covered in a subsequent publication, using the basic formalism derived here.

The quantum treatments of propagation through an absorbing and dispersive dielectric slab and the description of the quantum states of incident N-photon and coherent pulses are summarized in Sec. II. The properties of the transmitted pulse are calculated in Sec. III, where it is shown that the pulse suffers apparent delay or acceleration and broadening or narrowing, depending on the values of the slab and pulse parameters. The nature of the thermal radiation emitted by the slab itself is determined in Sec. IV. The conclusions of the work are summarized in Sec. V.

II. SLAB FIELDS AND POYNTING VECTOR

In this section we derive a general expression for the power density of a quantized electromagnetic field after propagation through a bounded dielectric that shows both loss and dispersion. We also consider the forms of the quantum states for N-photon and coherent pulses.

The form of the dielectric function for a slab of thickness $2l$ is

$$\epsilon(x,\omega)=\begin{cases}\epsilon(\omega)=n^2(\omega)=[\eta(\omega)+i\kappa(\omega)]^2 & \text{for } |x|\leqslant l\\ 1 \quad \text{for } |x|\geqslant l,\end{cases} \tag{2.1}$$

where the complex refractive index $n(\omega)$ is assumed to be a known function, which is related to the real refractive index $\eta(\omega)$ and extinction coefficient $\kappa(\omega)$, defined for positive frequencies. The electromagnetic field is quantized on the basis of a continuous set of modes propagating in the direction perpendicular to the surface of the slab so that waves propagate in the direction of the positive x axis with their transverse electric and magnetic vector operators $\hat{\mathbf{E}}(x,t)$ and $\hat{\mathbf{B}}(x,t)$ parallel to the y and z axes, respectively. The schematic arrangement of the propagation geometry for the vari-

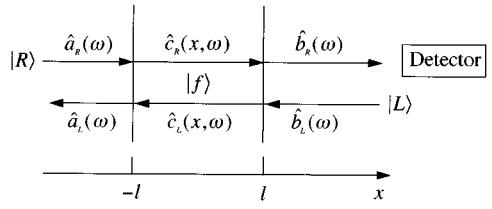

FIG. 1. Spatial configuration of the dielectric slab and notation for the destruction operators used in the definition of the relevant electric fields.

ous components of the field given in Fig. 1 shows the notation for the slab input and output field operators.

The vector potential operator $\hat{\mathbf{A}}(x,t)$ can be obtained by using standard Green-function methods to solve the relevant Maxwell equations [2]. In the scattering region $x>l$ its positive frequency component is

$$\hat{A}^{(+)}(x,t)=\int_0^\infty d\omega\sqrt{(\hbar/4\pi\epsilon_0 c\omega S)}\times[\hat{b}_R(\omega)e^{i\omega x/c}+\hat{b}_L(\omega)e^{-i\omega x/c}]e^{-i\omega t}, \tag{2.2}$$

where S is the area of quantization in the yz plane. The operator for the rightward-propagating outgoing field is given in terms of the leftward and rightward input fields by

$$\hat{b}_R(\omega)=R(\omega)\hat{b}_L(\omega)+T(\omega)\hat{a}_R(\omega)+\hat{F}(\omega), \tag{2.3}$$

where

$$T(\omega)=\frac{4n(\omega)}{D(\omega)}e^{2i\omega[n(\omega)-1]l/c}=4n(\omega)\exp\{2i\omega[n(\omega)-1](l/c)-\ln D(\omega)\} \tag{2.4}$$

and

$$R(\omega)=\frac{[n^2(\omega)-1]}{D(\omega)}e^{-2i\omega l/c}[e^{4i\omega n(\omega)l/c}-1], \tag{2.5}$$

with

$$D(\omega)=[n(\omega)+1]^2-[n(\omega)-1]^2\exp[4i\omega n(\omega)l/c], \tag{2.6}$$

are the complex amplitudes of the transmission and reflection coefficients, respectively. The second form of the transmission coefficient in Eq. (2.4) is useful for Sec. III.

The operator $\hat{F}(\omega)$ in Eq. (2.3) represents the noise associated with the dissipation in the slab, and its form is given by

$$\hat{F}(\omega)=i\sqrt{2\omega\eta(\omega)\kappa(\omega)/c}\int_{-l}^{l}dx[V(\omega)e^{-i\omega n(\omega)x/c}+W(\omega)e^{i\omega n(\omega)x/c}]\hat{f}(x,\omega), \tag{2.7}$$

where

$$V(\omega)=2[n(\omega)+1]\exp\{i\omega[n(\omega)-1]l/c\}D^{-1}(\omega),\qquad W(\omega)=2[n(\omega)-1]\exp\{i\omega[3n(\omega)-1]l/c\}D^{-1}(\omega), \tag{2.8}$$

and the $\hat{f}(x,\omega)$ are spatially distributed Langevin noise current operators with the commutation relation

$$[\hat{f}(x,\omega),\hat{f}^\dagger(x',\omega')]=\delta(x-x')\delta(\omega-\omega'). \tag{2.9}$$

The strength of the noise operator $\hat{F}(\omega)$ is proportional to the square-root of the extinction coefficient $\kappa(\omega)$, and it vanishes for a lossless dielectric. The input and output operators in Eq. (2.3) satisfy the boson commutation relations

$$[\hat{b}_R(\omega),\hat{b}_R^\dagger(\omega')]=[\hat{b}_L(\omega),\hat{b}_L^\dagger(\omega')]=[\hat{a}_R(\omega),\hat{a}_R^\dagger(\omega')]=\delta(\omega-\omega'),\qquad [\hat{a}_R(\omega),\hat{b}_L^\dagger(\omega')]=0, \tag{2.10}$$

and their consistency is ensured by the noise operator commutator

$$[\hat{F}(\omega),\hat{F}^\dagger(\omega')]=[1-|R(\omega)|^2-|T(\omega)|^2]\delta(\omega-\omega'), \tag{2.11}$$

which is readily verified with the use of Eqs. (2.7)–(2.9).

The electric and magnetic fields are derived from the quantized vector potential,

$$\hat{E}(x,t)=-\partial\hat{A}(x,t)/\partial t,\qquad \hat{B}(x,t)=\partial\hat{A}(x,t)/\partial x, \tag{2.12}$$

and the average Poynting vector is calculated according to

$$\langle\hat{S}(x,t)\rangle=\mu_0^{-1}\langle f|\langle L|\langle R|\hat{E}(x,t)\hat{B}(x,t)|R\rangle|L\rangle|f\rangle. \tag{2.13}$$

The expectation value is over a product state that comprises the states of the field impinging leftwards $|L\rangle$ and rightwards $|R\rangle$ on the slab. The state of the reservoir that accounts for dissipation within the slab is a statistical mixture, which we represent symbolically by $|f\rangle$. We specifically take the incoming state $|L\rangle$ to be a conventional vacuum, $|0\rangle$, and the quantized field $|R\rangle$ impinging from the left is taken as a photon-number state, denoted by $|N,\xi\rangle$. The normal-order Poynting vector on the right of the slab obtained from Eq. (2.13) then simplifies to

$$\langle{:}\hat{S}(x,t){:}\rangle=\frac{\hbar}{2\pi S}\int_0^\infty d\omega\int_0^\infty d\omega'\sqrt{\omega\omega'}e^{-i(\omega-\omega')(t-x/c)}\times\langle f|\langle 0|\langle N,\xi|\hat{b}_R^\dagger(\omega)\hat{b}_R(\omega')|N,\xi\rangle|0\rangle|f\rangle. \tag{2.14}$$

The photon-number state can be generated with the use of a quantum operator acting on the vacuum, of the form [14]

$$|N,\xi\rangle=\frac{1}{\sqrt{N!}}\left[\int_0^\infty d\omega\xi^*(\omega)\hat{a}_R^\dagger(\omega)\right]^N|0\rangle. \tag{2.15}$$

The normalized function $\xi(\omega)$ describes the frequency distribution of the N-photon wave packet, whose form is deter-

mined by the way in which the photon state is prepared. We consider here a wave packet with a Gaussian frequency distribution centered on ω_c (carrier) and a mean-square spatial length $\mathcal{L}^2$,

$$\xi(\omega)=\left(\frac{\mathcal{L}^2}{2\pi c^2}\right)^{1/4}\exp[-\mathcal{L}^2(\omega-\omega_c)^2/4c^2], \quad (2.16)$$

where the frequency spread of the wave packet is $c/\mathcal{L}$. The Fourier time transform of Eq. (2.16) represents a pulse whose peak would pass the origin of coordinates at time $t=0$ in the absence of the dielectric slab. Single-photon states with Gaussian wave packets can be realized experimentally [15]. It is sometimes useful to compare these states with an incident pulse in the form of a coherent state defined by [14]

$$|\{\alpha(\omega)\}\rangle=\hat{D}(\{\alpha(\omega)\})|0\rangle \equiv\exp\left\{\int d\omega[\alpha(\omega)\hat{a}_R^{\dagger}(\omega)-\alpha^*(\omega)\hat{a}_R(\omega)]\right\}|0\rangle, \quad (2.17)$$

where a Gaussian pulse with mean photon number $\overline{N}$ is obtained by taking

$$\alpha(\omega)=\overline{N}^{1/2}\xi(\omega), \quad (2.18)$$

with $\xi(\omega)$ defined in Eq. (2.16). The quantum-mechanical coherent state (2.17) shows similar behavior to a classical pulse. The photon-number state (2.15) has no classical analogue; it shows classical-type behavior in terms of its first-order coherence and the propagation of its power density, but it displays characteristic nonclassical behavior in terms of its higher-order coherence and correlation properties.

The dielectric slab is assumed to be maintained at a finite-temperature T, and the Langevin noise current operators have the expectation values

$$\langle f|\hat{f}(x,\omega)|f\rangle=\langle f|\hat{f}(x,\omega)\hat{f}(x',\omega')|f\rangle=0,$$
$$\langle f|\hat{f}^{\dagger}(x,\omega)\hat{f}(x',\omega')|f\rangle=\overline{n(}\omega,T)\,\delta(x-x')\,\delta(\omega-\omega'), \quad (2.19)$$

where

$$\overline{n(}\omega,T)=[e^{\hbar\omega/kT}-1]^{-1} \quad (2.20)$$

is the mean number of thermal photons at frequency ω. The temperature determines the level of excitation of the noise currents. The free-space regions surrounding the slab are assumed to be at zero temperature.

With the help of Eqs. (2.15), (2.16), and (2.19), the average normal-order Poynting vector Eq. (2.14) for an N-photon Gaussian wave packet after transmission through the slab can be written as

$$\langle:\hat{S}(x,t):\rangle\equiv\langle:\hat{S}:\rangle_{pl}+\langle:\hat{S}:\rangle_{sl} =2\epsilon_0 c\left[N\left|J_1\left(t-\frac{x}{c}\right)\right|^2+J_2(0)\right], \quad (2.21)$$

where

$$J_1(q)\equiv\sqrt{\hbar/4\pi\epsilon_0 cS}\int_0^{\infty}d\omega e^{-i\omega q}\omega^{1/2}T(\omega)\xi(\omega) \quad (2.22)$$

and

$$J_2(q)\equiv\frac{\hbar}{2\pi\epsilon_0 c^2 S}\int_0^{\infty}d\omega e^{-i\omega q}\omega^2\eta(\omega)\kappa(\omega)\overline{n(}\omega,T) \times\int_{-l}^{l}dx|V(\omega)e^{-i\omega n(\omega)x/c}+W(\omega)e^{i\omega n(\omega)x/c}|^2. \quad (2.23)$$

The average Poynting vector thus separates into two contributions: the part $\langle:\hat{S}:\rangle_{pl}$ depends on the position and time, and on the parameters of the incident pulse and the slab, while the part $\langle:\hat{S}:\rangle_{sl}$ is independent of position, time, and the pulse characteristics, and only depends on the slab parameters. The pulse power density transmitted through the slab and the noise power density radiated by the slab itself can thus be analyzed separately.

III. PULSE TRANSMISSION

In order to characterize the propagation through the absorbing slab of the energy stored in a quantized electromagnetic field, an explicit expression for the first contribution to the Poynting vector in Eq. (2.21) is needed. The relevant integral J_1 is difficult to perform in general; however, an analytic result can be derived with the help of realistic assumptions.

First, we take the frequency spread of the photon-number wave packet to be much smaller than the carrier frequency,

$$c/\mathcal{L}\ll\omega_c. \quad (3.1)$$

The lower bound in the integral can then be replaced by $-\infty$ and $\langle:\hat{S}:\rangle_{pl}$ reduces to

$$\langle:\hat{S}:\rangle_{pl}=\sqrt{\frac{\mathcal{L}^2}{2\pi c^2}}\frac{N\hbar\omega_c}{2\pi S}\left|\int_{-\infty}^{\infty}d\Omega T(\omega_c+\Omega) \times e^{-i\Omega(t-x/c)}e^{-\mathcal{L}^2\Omega^2/4c^2}\right|^2, \quad (3.2)$$

where the square-root frequency factor in the integrand of J_1 in Eq. (2.21) is replaced by $\sqrt{\omega_c}$. We have also changed the variable of integration to $\Omega=\omega-\omega_c$. When $T(\omega_c+\Omega)$ is set equal to unity, Eq. (3.2) yields the normal-order Poynting vector associated with the incident pulse, which can be straightforwardly evaluated as

$$\langle:\hat{S}:\rangle_{\rm inc}=S_0 e^{-2(x-ct)^2/\mathcal{L}^2}, \quad (3.3)$$

where

$$S_0=\sqrt{(2/\pi)}\,\frac{Nc\hbar\omega_c}{\mathcal{L}S} \quad (3.4)$$

is the peak power density of the incident pulse.

Second, for a slab with a reasonably smooth dielectric function (no optical band-gap edge, no singularities, etc.)

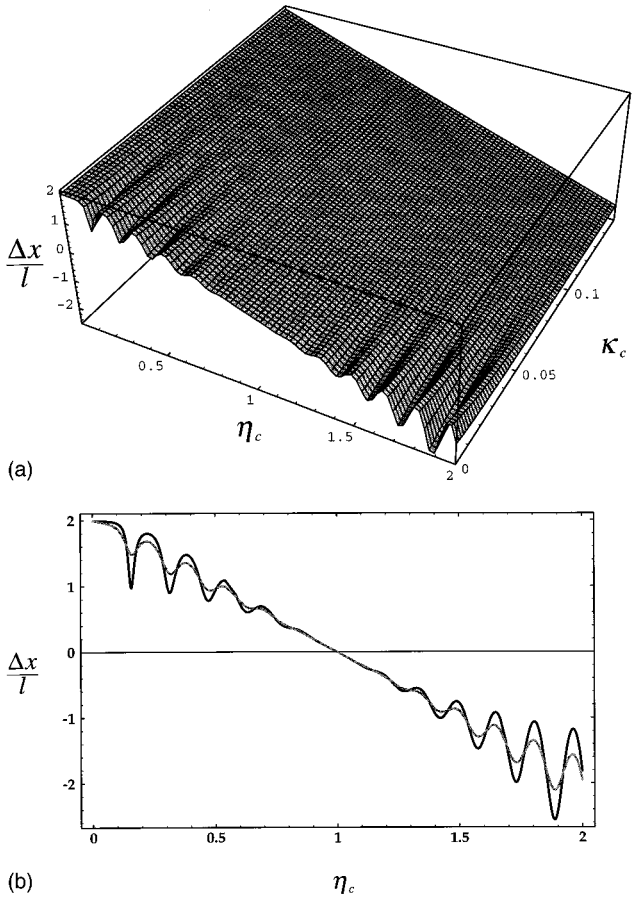

FIG. 2. Shift in the peak position of a Gaussian pulse transmitted through a slab of thickness $2l$ relative to free-space propagation in units of l as a function of the medium real refractive index η_c and extinction coefficient κ_c. Dispersion is neglected. The film thickness and carrier frequency satisfy $\omega_c l/c=10$ and the incident pulse width is $\mathcal{L}=40l$. (a) complete variation and (b) variation with η_c for $\kappa_c=0$ (black curve) and $\kappa_c=0.02$ (grey curve).

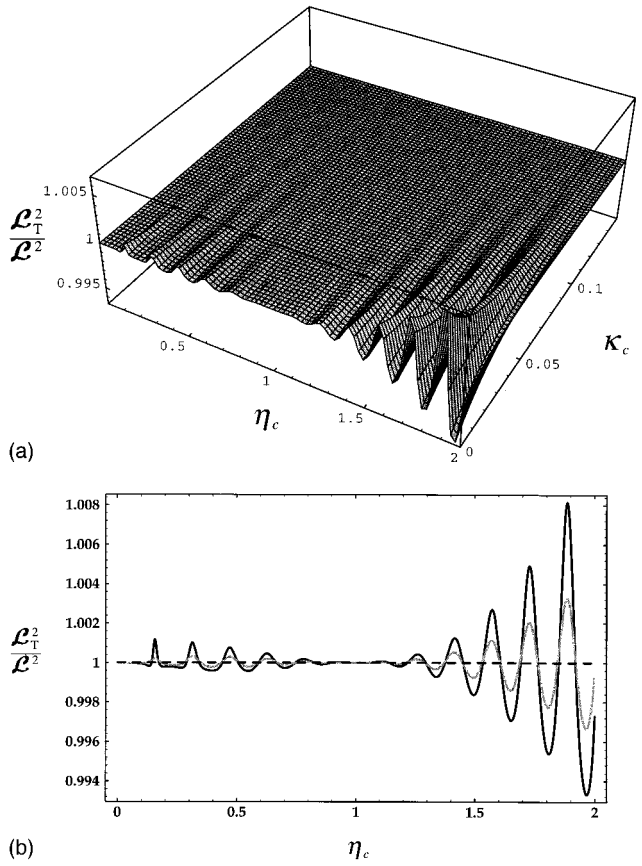

FIG. 3. Mean-square length of the transmitted Gaussian pulse for the same parameters as in Fig. 2, in units of the incident mean-square length $\mathcal{L}^2$ (a) complete variation and (b) variation with η_c for $\kappa_c=0$ (black curve) and $\kappa_c=0.02$ (grey curve).

$n(\omega)$, $\eta(\omega)$, and $\kappa(\omega)$ vary slowly over the narrow bandwidth $c/\mathcal{L}$ of the pulse. The optical wave vector can thus be expanded around the pulse carrier frequency ω_c in the usual way,

$$k(\omega)\equiv\frac{\omega n(\omega)}{c}=k(\omega_c)+\left.\frac{\partial k(\omega)}{\partial\omega}\right|_{\omega_c}(\omega-\omega_c)+\frac{1}{2}\left.\frac{\partial^2 k(\omega)}{\partial\omega^2}\right|_{\omega_c}(\omega-\omega_c)^2+\cdots\cong k_c+k_c'\Omega=k_c+(k_{cr}'+ik_{ci}')\Omega, \tag{3.5}$$

where the second and higher-order terms in the expansion are neglected, $k_c=\omega_c n_c/c$ and $n_c=n(\omega_c)$. The prime denotes the frequency derivative in the linear term and this is divided into its real and imaginary parts in the final step, where the real part is related to the group velocity v_g according to $k_{cr}'=1/v_g$.

Third, we take the incident pulse to be much longer than the optical thickness of the slab,

$$\mathcal{L}\gg 2l\eta_c/\pi, \tag{3.6}$$

so that the transmitted light retains the form of a single pulse. The form of the transmitted pulse is more complicated when Eq. (3.6) is not satisfied, and it exhibits breakup into a series of distinct pulses in the limit where the incident pulse is much shorter than the slab thickness [16] (a similar pulse breakup is observed in transmission through a Fabry-Perot cavity [17]). When Eq. (3.6) is satisfied, it is appropriate to make an expansion of the logarithmic term in $T(\omega_c+\Omega)$ correct to the second order in $\Omega l k_c'$. This leads with the use of Eq. (3.5) and the second form of the transmission coefficient in Eq. (2.4) to

$$T(\omega_c+\Omega)=T(\omega_c)\exp\left\{2i\left[k_c'-\frac{1}{c}+\frac{2k_c'(n_c-1)^2}{D(\omega_c)}\exp\left(\frac{4i\omega_c n_c l}{c}\right)\right]\Omega l-\frac{8k_c'^2(n_c^2-1)^2}{D^2(\omega_c)}\exp\left(\frac{4i\omega_c n_c l}{c}\right)\Omega^2 l^2\right\}, \tag{3.7}$$

where $D(\omega)$ is defined in Eq. (2.6). The coefficients of Ω and Ω^2 are complex; one should notice particularly the decaying and the oscillating components, respectively, in Ω and Ω^2.

The form of the transmitted pulse power density is now obtained by substitution of Eq. (3.7) into the integrand in Eq. (3.2). The integral can be performed analytically, but the result is complicated and the full details are given in the Appendix. The transmitted pulse retains a Gaussian shape, given by the analytic expression of Eq. (A2), but the natures of the variations in the pulse peak position and pulse length are not very transparent. Figure 2 thus illustrates how the shift Δx in the position of the peak of the transmitted pulse varies as a function of η_c and κ_c after propagating through a slab whose thickness is much smaller than the incident pulse length. We specifically plot the third and fourth term in the square bracket of the numerator of Eq. (A2). The shift oscillates as a function of η_c around a mean value that decreases monotonically with increasing η_c, and the amplitude of the oscillations increases with $|\eta_c-1|$. For the parameters used in this figure the maximum shift is of the order of a slab thickness. The oscillations damp out with increasing extinction coefficient κ_c. Likewise in Fig. 3 we illustrate the variations in the transmitted pulse length for the same situation as Fig. 2; here we plot the expression in the curly bracket in the denominator of Eq. (A2) that represents the deviation of the mean-square length $\mathcal{L}_T^2$ from its incident value $\mathcal{L}^2$. The transmission through an absorbing slab may shorten or lengthen the pulse depending on the value of the real refractive index η_c, particularly for large η_c's. The relative change in the pulse length is of the order of a fraction of a percent. Increasing absorption again damps the oscillations out and the pulse length is unchanged from its incident value for sufficiently large κ_c. Dispersion in the refractive index $\eta(\omega)$ around its value η_c and in the extinction coefficient $\kappa(\omega)$ around its value κ_c at the carrier frequency, which are included in the general results of the Appendix, are neglected in both Figs. 2 and 3, i.e., we set the usual group velocity ν_g evaluated at the carrier frequency equal to the corresponding phase velocity,

$$k'_{cr}\equiv\frac{1}{\nu_g}=\frac{\eta_c}{c}+\frac{\omega_c}{c}\left.\frac{\partial\eta(\omega)}{\partial\omega}\right|_{\omega_c}\rightarrow\frac{\eta_c}{c} \tag{3.8}$$

and

$$k'_{ci}=\frac{\kappa_c}{c}+\frac{\omega_c}{c}\left.\frac{\partial\kappa(\omega)}{\partial\omega}\right|_{\omega_c}\rightarrow\frac{\kappa_c}{c} \tag{3.9}$$

to avoid the introduction of a further arbitrary parameter.

Relatively simple expressions for the transmitted Poynting vector are obtained in limiting special cases, and the simplest of these is that of zero absorption, $\kappa_c=0$. The integration in Eq. (2.22) can be performed without too much difficulty in this case, and the transmitted Poynting vector of the pulse has the Gaussian form

$$\langle:\hat{S}_{\kappa_c=0}:\rangle_{pl}=S_T e^{-2(x-ct-\Delta x)^2/\mathcal{L}_T^2}, \tag{3.10}$$

where the spatial shift in the position of the peak of the pulse from its value ct in the absence of the slab is given by

$$\Delta x=2l-\frac{2lc}{\nu_g}\frac{8\eta_c(\eta_c^2+1)}{(\eta_c+1)^4+(\eta_c-1)^4-2(\eta_c^2-1)^2\cos(4\omega_c\eta_c l/c)} \tag{3.11}$$

and its mean-square spatial length is given by

$$\mathcal{L}_T^2=\mathcal{L}^2+\frac{32l^2c^2}{\nu_g^2}\frac{(\eta_c^2-1)^2\{[(\eta_c+1)^4+(\eta_c-1)^4]\cos(4\omega_c\eta_c l/c)-2(\eta_c^2-1)^2\}}{[(\eta_c+1)^4+(\eta_c-1)^4-2(\eta_c^2-1)^2\cos(4\omega_c\eta_c l/c)]^2}. \tag{3.12}$$

These expressions are correct to the second order in $l/\mathcal{L}$, and Eq. (3.11) is consistent with an expression for the apparent velocity of propagation of a pulse through a slab derived previously [6]. We do not give the explicit expression for the peak power density S_T of the transmitted pulse. The black curves in Figs. 2(b) and 3(b), respectively, show the forms of the peak shift Eq. (3.11) and the transmitted pulse length Eq. (3.12) for zero absorption. The peak shift oscillates around a mean value that is found by taking an average of Eq. (3.11) over a period of the cosine to be

$$\overline{\Delta x}=2l\left(1-\frac{c}{\nu_g}\right); \tag{3.13}$$

this is the value expected for the change in effective path length caused by the propagation of the peak of the pulse with velocity ν_g, in agreement with previous calculations [3,6,7]. The mean-square length oscillates around a mean value that is obtained from Eq. (3.12) as unchanged from the incident value,

$$\overline{\mathcal{L}_T^2}=\mathcal{L}^2. \tag{3.14}$$

The oscillations can be understood by consideration of further specializations of the system parameters. Thus if the carrier frequency and slab thickness satisfy

$$2\omega_c\eta_c l/c=\pi n \quad (n=\text{integer}), \tag{3.15}$$

the shift Eq. (3.11) in the spatial position of the peak of the pulse can be decomposed as

$$\Delta x=2l-l\frac{c}{\nu_g}\frac{\eta_c^2+1}{\eta_c}=2l\left(1-\frac{c}{\nu_g}\right)-l\frac{c}{\nu_g}\frac{(\eta_c-1)^2}{\eta_c}. \tag{3.16}$$

The first term on the right results from pulse propagation through the slab with the group velocity and for $\nu_g>0$ the second term results from an enhancement of the rear of the pulse by the constructive interference of in-phase contributions from multiple reflections inside the slab. The length expression (3.12) reduces to

$$\mathcal{L}_T^2=\mathcal{L}^2+\frac{2l^2c^2}{\nu_g^2}\frac{(\eta_c^2-1)^2}{\eta_c^2}, \tag{3.17}$$

where the increase in pulse length is caused by the same interference effects. The integrated area of the transmitted pulse is unchanged from that of the incident pulse as 100% transmission occurs when the condition (3.15) is satisfied. The results for this special case agree with earlier work [16] if dispersion is neglected.

Simple results also occur for

$$2\omega_c\eta_c l/c=\pi n/2 \quad (n=\text{odd integer}). \tag{3.18}$$

The shift in the spatial position Eq. (3.11) of the peak of the pulse is now decomposed as

$$\Delta x=2l-\frac{2lc}{\nu_g}\frac{2\eta_c}{\eta_c^2+1}=2l\left(1-\frac{c}{\nu_g}\right)+\frac{2lc}{\nu_g}\frac{(\eta_c-1)^2}{\eta_c^2+1}, \tag{3.19}$$

where the first and second terms on the right again represent the effects of the change in the velocity of transmission through the slab and the multiple reflections inside the slab, respectively. The multiple reflections now produce a *positive* contribution to the shift for $\nu_g>0$, corresponding to an apparent speeding up of the pulse. This effect is caused by the opposite phases of the multiply reflected waves when the condition (3.18) is satisfied, so that the rear part of the transmitted pulse is diminished by destructive interference. The length expression (3.12) reduces to

$$\mathcal{L}_T^2=\mathcal{L}^2-\frac{8l^2c^2}{\nu_g^2}\frac{(\eta_c^2-1)^2}{(\eta_c^2+1)^2}, \tag{3.20}$$

where the reduction in the mean-square length of the pulse is another consequence of the same interference. The integrated area of the transmitted pulse is now reduced from that of the incident pulse by the transmission factor appropriate to the condition (3.18).

The analytical results in the previous two paragraphs provide simple examples of the ways in which apparent ''superluminal'' behavior with $\Delta x>0$ can occur in pulse transmission through a dielectric slab. The first terms on the right in Eqs. (3.16) and (3.19) represent the bulk effect of transmission across the slab at the group velocity, and these terms are positive if $\nu_g>c$ or $\nu_g<0$ [3,4]. The second terms on the right of Eqs. (3.16) and (3.19) represent surface effects caused by multiple reflections inside the slab, and these terms can be positive or negative, depending on the slab thickness and the sign of the group velocity. The multiple reflections may make an important contribution to the superluminal behavior, although such effects occur in more striking form for multilayer dielectric films [10–13] rather than the single dielectric slab considered here. For $\nu_g<0$, both Eqs. (3.16) and (3.19) give $\Delta x>0$, while for $\nu_g>0$, the transmission is superluminal with $\Delta x>0$ for the condition expressed by Eq. (3.18) only when

$$\frac{\nu_g}{c}>\frac{2\eta_c}{\eta_c^2+1}. \tag{3.21}$$

In the absence of dispersion, when the group velocity equals the phase velocity as in Eq. (3.8), superluminal transmission with $\Delta x>0$ is predicted both by Eqs. (3.16) and (3.19) when $\eta_c<1$, and this behavior is evident in Fig. 2; subluminal transmission occurs for $\eta_c>1$. The Gaussian pulse adopted here maintains its functional form on transmission through the slab, and the position of its peak provides a simple measure of any apparent delay or speeding up, without the need for any justification of a choice from the range of definitions of traversal times [10]. It should be emphasized that in all cases, the value of the transmitted Poynting vector at the leading edge of the pulse is smaller than its value in the absence of the slab and Einstein causality is never violated.

Another special case occurs in the presence of absorption, $\kappa_c\neq 0$, but with the assumption that the condition (3.15) for near transparency of the slab is satisfied. With the help of the condition (3.6) and the result (3.7), the integral in Eq. (3.2) can now be performed (§3.923 of [18]) and one gets after some effort

$$\langle:\hat{S}:\rangle_{pl}=S_0\mathcal{I}\exp\left\{-\frac{2\{ct-x-l\beta_2-[l\alpha_2\beta_1\kappa_c^2/\alpha_1+(\mathcal{L}/2l)^2]\}^2}{\mathcal{L}^2+4l^2\{\alpha_1+[\beta_1^2\kappa_c^2/\alpha_1+(\mathcal{L}/2l)^2]\}}\right\}, \tag{3.22}$$

where

$$\mathcal{I}=\frac{16|n_c|^2\{(\beta_1\kappa_c)^2+[\alpha_1+(\mathcal{L}/2l)^2]^2\}^{-1/2}}{(2l/\mathcal{L})^2\Delta_{c-}^2}\times\exp\left\{\frac{\kappa_c^2\alpha_2^2/2}{\alpha_1+(\mathcal{L}/2l)^2}\right\} \tag{3.23}$$

determines how the peak incident intensity scales through the slab, and α_1, α_2, β_1, and β_2 are dimensionless pulse and material-dependent parameters defined as

$$\alpha_1=8c^2k_{cr}'^2\frac{(\eta_c^2-1)^2}{\Delta_{c-}^2}, \tag{3.24}$$

$$\beta_1=16c^2k_{cr}'(\eta_c^2-1)\frac{2k_{cr}'(\Delta_{c+}/\Delta_{c-})+(\eta_c^2-1)(k_{ci}'/\kappa_c)}{\Delta_{c-}^2}, \tag{3.25}$$

$$\alpha_2 = 2c\,\frac{8k'_{cr}(\eta_c^2-1)+(k'_{ci}/\kappa_c)\Delta_{c+}\Delta_{c-}}{\Delta_{c-}^2}, \qquad (3.26)$$

and

$$\beta_2 = -2+2ck'_{cr}(\Delta_{c+}/\Delta_{c-}) \qquad (3.27)$$

with

$$\Delta_{c\pm} = (\eta_c+1)^2 e^{2\omega_c\kappa_c l/c} \pm (\eta_c-1)^2 e^{-2\omega_c\kappa_c l/c}. \qquad (3.28)$$

The transmitted light again maintains the appearance of a Gaussian pulse, but its strength, position, and length are modified by quite complicated functions of the pulse and material parameters.

For values of the extinction coefficient corresponding to a weak absorbing regime the parameter $\kappa_c\omega_c l/c$ is generally small and it is much less than unity for many experimental conditions. Then α_1, α_2, β_1, and β_2 can be expanded in terms of this perturbation parameter and the corresponding Poynting vector expectation value in Eq. (3.22) leads to the following expressions for the shift in the spatial position of the peak of the pulse,

$$\Delta x = 2l - l\,\frac{c}{\nu_g}\,\frac{(\eta_c^2+1)}{\eta_c} + l\,\frac{c}{\nu_g}\,\frac{(\eta_c^2-1)^2}{\eta_c^2}\,\kappa_c\,\frac{\omega_c l}{c} \qquad (3.29)$$

and the mean-square pulse length,

$$\mathcal{L}_T^2 = \mathcal{L}^2 + 2l^2\,\frac{c^2}{\nu_g^2}\,\frac{(\eta_c^2-1)^2}{\eta_c^2} - 4l^2\,\frac{c^2}{\nu_g^2}\,\frac{(\eta_c^2-1)^2(\eta_c^2+1)}{\eta_c^3}\,\kappa_c\,\frac{\omega_c l}{c}, \qquad (3.30)$$

to first order in $\kappa_c\omega_c l/c$ with $k'_{cr}=1/\nu_g$. It is seen that for $\nu_g>0$ the shift in the peak of the pulse is increased and the mean-square pulse length is reduced with respect to the values associated with the nonabsorbing regime examined above, respectively, Eqs. (3.16) and (3.17). These changes occur because the contributions of the multiple reflections to the peak shift and pulse width are progressively diminished by the effects of the attenuation.

On the other hand, for values of the extinction coefficient corresponding to strong absorption $\kappa_c\omega_c l/c$ is larger than or at least equal to unity for typical experimental conditions; the coefficients α_1, α_2, β_1, and β_2 can be expanded within this limit when only β_2 remains non-negligible and the Poynting vector (3.22) reduces to

$$\langle{:}\hat{S}{:}\rangle_{pl} = S_0\mathcal{I}\,\exp(-2\{ct-x-2l[(c/\nu_g)-1]\}^2/\mathcal{L}^2). \qquad (3.31)$$

The strong absorption completely quenches the effects of the multiple reflections in the slab, so that the shift in peak position is merely the contribution from the optical thickness of the slab and the pulse length is unchanged from the incident pulse. These behaviors are seen in the high κ_c regimes of Figs. 2(a) and 3(a), respectively. Of course, the peak intensity $\mathcal{I}$ is extremely small in this limit, but the form of Eq. (3.31) illustrates the physical effects of the high absorption on the pulse shape.

The results of this section provide an extension of recent work [16] on the propagation of a quantized field through a slab with constant and real refractive index. It is important to point out that the effects discussed above also occur in the propagation of the coherent pulse $|\{\alpha(\omega)\}\rangle$ described by Eqs. (2.17) and (2.18) through a dielectric slab. Identical expressions are obtained for the transmitted Poynting vector in this case, within approximations that are valid when the inequalities (3.1) and (3.6) apply, and the same results survive in the classical limit [6]. However, the quantum-mechanical formalism presented here can also be used to determine the higher-order propagation characteristics of optical pulses with nonclassical features, which are not accessible by any classical theory.

IV. SLAB RADIATION

We now proceed to examine the second contribution in Eq. (2.21) coming from the intensity radiated by the slab alone. This contribution is determined by the properties of the noise operator $\hat{F}(\omega)$ defined in Eq. (2.7). Using the forms (2.8) of the coefficients $V(\omega)$ and $W(\omega)$, the spatial integral in J_2 defined by Eq. (2.23) can readily be carried out to obtain

$$\begin{aligned}\langle{:}\hat{S}{:}\rangle_{sl} &= \int_0^\infty d\omega\,\frac{\hbar\omega}{\pi S}\,\overline{n}(\omega,T)\Bigg\{\eta(\omega)[|V(\omega)|^2+|W(\omega)|^2] \\ &\quad\times\sinh\left(\frac{2\omega\kappa(\omega)l}{c}\right)+\kappa(\omega)[V(\omega)W^*(\omega) \\ &\quad+V^*(\omega)W(\omega)]\sin\left(\frac{2\omega\eta(\omega)l}{c}\right)\Bigg\} \\ &\equiv \int_0^\infty d\omega\langle{:}\hat{S}(\omega){:}\rangle_{sl}. \end{aligned} \qquad (4.1)$$

This clearly vanishes in the limits $l\to 0$, when the slab is essentially removed, in the limit $\kappa(\omega)\to 0$, when the strength of the noise operator $\hat{F}(\omega)$ tends to zero, and at zero temperature, when the slab radiation disappears altogether. An analytic expression for the integral in Eq. (4.1) is, in general, very difficult owing to the intricate oscillating behavior of $D(\omega)$ in the denominators of $V(\omega)$ and $W(\omega)$. Magnitudes of the slab Poynting vector, however, can be obtained numerically and from Eq. (4.1) we find, e.g., that for the characteristic values of $\eta=2.85$, an extinction coefficient $\kappa=3\times10^{-4}$ and $l=10^{-3}$ m, $\langle{:}\hat{S}{:}\rangle_{sl}/(\hbar c^2/2\pi S l^2)$ varies in the range $8\times10^{-3}\leftrightarrow 6\times10^{3}$ for temperatures between 3 and 300 K, respectively.

Equation (4.1) usefully provides a direct expression for the Poynting vector spectrum $\langle{:}\hat{S}(\omega){:}\rangle_{sl}$ of the electromagnetic field emitted by a lossy and dispersive dielectric at finite temperature. Typical values of the extinction coefficient are very much less than unity and we shall regard $\kappa(\omega)$ as an expansion parameter throughout the following discussion. Because the second contribution in Eq. (4.1) is much

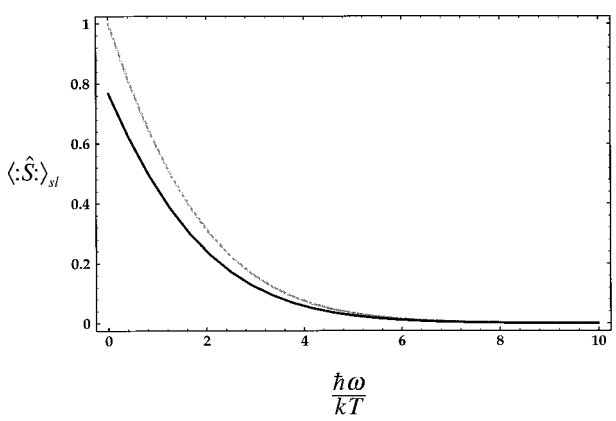

FIG. 4. Poynting vector spectrum Eq. (4.2) in units of $kT/2\pi S$ as a function of $\hbar\omega/kT$ for a *thick* lossy slab of width $2l$ at finite temperature T such that $l \cong 10^8 \hbar c/kT$. The imaginary part of the refractive index is $\kappa = 3\times10^{-4}$ and the real part is $\eta = 2.85$ (black curve) and $\eta = 1$ (grey curve).

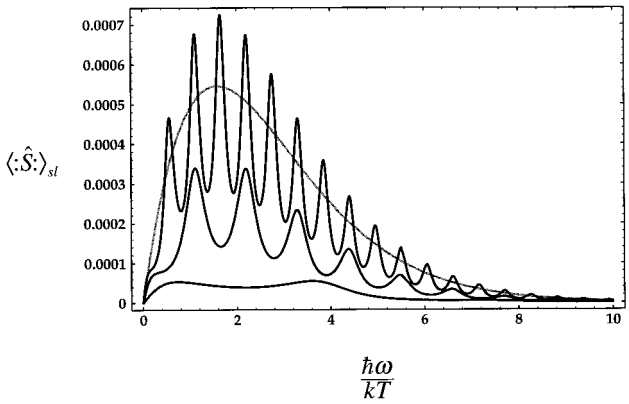

FIG. 5. Poynting vector spectrum Eq. (4.2) in units of $kT/2\pi S$ as a function of $\hbar\omega/kT$ for a *thin* lossy slab with $\eta = 2.85$ and $\kappa = 3\times10^{-4}$. The temperature and the slab width satisfy $l = \hbar c/kT$, $l = \hbar c/2kT$, and $l = \hbar c/7kT$, respectively, from the top down (black curves). The grey curve refers to the parameters $l = \hbar c/0.7kT$, $\eta = 1$, and $\kappa = 3\times10^{-4}$.

smaller than the first for most reasonable ranges of parameters, we can rewrite the spectrum simply as

$$\langle :\hat{S}(\omega): \rangle_{\rm sl} = \frac{\hbar\omega}{\pi S}\,\overline{n(}\omega, T)\,\eta(\omega)[|V(\omega)|^2 + |W(\omega)|^2] \times \sinh\left(\frac{2\omega\kappa(\omega)l}{c}\right) \quad [\kappa(\omega) \ll \eta(\omega)]. \tag{4.2}$$

In the limit of an infinitely thick slab, Eq. (4.2) reduces with the use of Eqs. (2.8) and (2.20) to

$$\langle :\hat{S}(\omega): \rangle_{\rm sl} \cong \frac{\hbar\omega}{2\pi S}\,\frac{1}{e^{\hbar\omega/kT}-1}\,\frac{4\,\eta(\omega)}{[\,\eta(\omega)+1]^2+[\,\kappa(\omega)]^2} \quad [\omega\kappa(\omega)l/c \gg 1], \tag{4.3}$$

whose behavior is shown in Fig. 4 as a function of the normalized energy $\hbar\omega/kT$. One should note the uniform exponential decay for large ω's and the nonvanishing value at $\omega = 0$. This latter feature contradicts a property of the spectral expression (4.2), which clearly vanishes at $\omega = 0$, and it is a consequence of taking the limit shown on the right of Eq. (4.3) before evaluating the spectrum at $\omega = 0$. In addition, the extinction coefficient must strictly vanish for zero frequency [19], but the constant value assumed here is sufficiently small that this requirement is violated to an insignificant extent.

In the case of a finite slab, the argument $\omega\kappa(\omega)l/c$ in the exponents that occur in Eq. (4.2) is less than unity for the parameter values assumed here and for the infrared and lower frequencies that are thermally excited at reasonable temperatures. The averaged Poynting vector spectrum can then be rewritten with the help of a Taylor series expansion, and including terms up to the leading order in $\kappa(\omega)$ and $\omega\kappa(\omega)l/c$ one obtains

$$\langle :\hat{S}(\omega): \rangle_{\rm sl} = \frac{\hbar\omega}{2\pi S}\,\frac{1}{e^{\hbar\omega/kT}-1}\,\frac{2\,\eta(\omega)[3\,\eta^2(\omega) - 2\,\eta(\omega) + 3]\omega\kappa(\omega)l/c}{[\,\eta^2(\omega)+1]^2 + 4[\omega\kappa(\omega)l/c][\,\eta(\omega)-1]^2(2\,\eta(\omega) - \{[\,\eta(\omega)+1]\,\sin[2\omega\,\eta(\omega)l/c]\}^2)} \quad [\omega\kappa(\omega)l/c \ll 1]. \tag{4.4}$$

In the special case of a unit real part of the refractive index, this cumbersome result reduces to

$$\langle :\hat{S}(\omega): \rangle_{\rm sl} = \frac{\hbar\omega}{2\pi S}\,\frac{1}{e^{\hbar\omega/kT}-1}\,\frac{2\omega\kappa(\omega)l}{c} \quad [\eta(\omega) = 1]. \tag{4.5}$$

The spectrum from Eq. (4.4) is shown in Fig. 5 for the same parameter values as Fig. 4 and for three different values of l. When compared to the previous result for an infinite slab in Eq. (4.3), two major differences appear. *First*, the linear increase from $\omega = 0$, followed by a maximum at intermediate ω's, contrasts with the uniform decaying behavior of the spectrum Eq. (4.3) for an infinite slab. The wider the slab, the steeper the slope with which the spectrum increases from $\omega = 0$. A steeper slope, in turn, shifts higher and higher spectral peaks toward the static region, so that the shape of the finite-slab spectrum tends towards that of the infinitely thick slab. Note however that the spectrum Eq. (4.3) for the infinitely thick slab is obtained by taking the limit shown by the inequality on the right of this equation, and the spectrum cannot be rederived from the finite-slab expression (4.4).

Also note the different decaying behaviors for large ω's, $\sim\omega\exp(-\hbar\omega/kT)$ and $\sim\omega^2\exp(-\hbar\omega/kT)$ when comparing, e.g., Eq. (4.3) for $\eta(\omega)=1$ with Eq. (4.5). All these features are well illustrated in Figs. 4 and 5. *Second*, note the presence of oscillations whose frequency and amplitude increase with the slab width. These oscillations arise from the trigonometric term in the denominator of Eq. (4.4) and only disappear when the real part of the refractive index becomes unity (cf. grey curve in Fig. 5). They physically originate from the interference between reflections of the radiation inside the bounded medium while the lack of oscillations for the finite slab described by Eq. (4.5) is physically due to the fact that for $\eta(\omega)\rightarrow 1$ and $\kappa(\omega)\ll 1$ the boundary reflections disappear and so do the oscillations. The absence of oscillations for the case of an infinite slab can likewise be explained by the absence of boundaries.

It is instructive to draw a comparison between our results and the spectrum of the mean Poynting vector obtained from first principles. Consider a one-dimensional (1D) electromagnetic field: the one-dimensional character of the field is necessary since in our case the wave vector varies only in the direction perpendicular to the slab surface. The number of modes per unit frequency and length is given by $1/\pi c$ when only a single polarization is detected. With an energy $\hbar\omega$ associated with each mode and a mean thermal excitation given by Eq. (2.20), the mean energy per unit frequency and length is given by the 1D Planck's law

$$\langle u(\omega)\rangle=\frac{\hbar\omega}{\pi c}\,\frac{1}{e^{\hbar\omega/kT}-1}. \tag{4.6}$$

The mean Poynting vector spectral component in each direction across a surface S then follows as,

$$\langle{:}\hat{S}(\omega){:}\rangle=\frac{c}{2S}\,\langle u(\omega)\rangle=\frac{\hbar\omega}{2\pi S}\,\frac{1}{e^{\hbar\omega/kT}-1}. \tag{4.7}$$

The Planck spectrum is valid for a black body, which can be modeled by the slab treated in this paper by choosing parameters for which all radiation falling on the slab from outside is absorbed and none is reflected or transmitted. It is seen from Eqs. (2.4) and (2.5) that these conditions are achieved by taking the limits

$$\begin{aligned}&\omega\kappa(\omega)l/c\rightarrow\infty \quad \text{(no transmission)},\\ &\kappa(\omega)\rightarrow 0 \quad \text{and} \quad \eta(\omega)\rightarrow 1 \quad \text{(no reflection)}\end{aligned} \tag{4.8}$$

in succession, and the infinitely thick slab spectrum Eq. (4.3) does indeed reduce to Eq. (4.7) when the second and third limits in Eq. (4.8) are taken. Equation (4.7) is also consistent with the photon flux derived for the thermal emission from an opaque section of waveguide [20]. The spectrum derived in Eq. (4.4), or in Eq. (4.3), has the additional merit of illustrating how the frequency dependence of the complex refractive index and the finite-slab thickness affect the Poynting vector spectrum of the radiation emitted by a bounded lossy and dispersive medium at finite temperature.

V. CONCLUSIONS

We have applied the quantized electromagnetic field theory developed for an absorbing and dispersive dielectric slab [2] to determine the effects of transmission on the properties of an incident Gaussian pulse. The pulse is taken as an N-photon state, for future use in calculations of the effects of transmission on the nonclassical properties of light, but for the linear properties derived here the same results are obtained for coherent pulses, including the classical limit of the quantum formalism. In agreement with previous calculations, the pulse propagates through the slab with the group velocity appropriate to the dielectric material [3]. The group velocity may be larger than c, or even negative, but Einstein causality is never violated as the value of the Poynting vector at the detector at a given time is always smaller than its value in the absence of the dielectric slab [12].

The transmitted light contains two contributions. The first of these is a modified version of the incident Gaussian pulse, whose peak position is generally advanced or retarded in comparison with that expected from the simple shift $2l[1-(c/v_g)]$ associated with the change in velocity of propagation in the interior of the slab [7]. The length of the transmitted pulse is correspondingly reduced or increased in comparison with that of the incident pulse. These modifications of the pulse shape are interpreted in terms of interference between the contributions to the transmitted pulse from light that travels through the slab with no reflections and light that suffers multiple reflections from the slab surfaces. Multiple reflections have been suggested [10] as an important mechanism in the explanation of the apparent superluminal propagation that occurs for multilayered structures. Apparent superluminal propagation is predicted for the single slab considered here when the group velocity is negative or when it is positive and greater than the lower limit specified in Eq. (3.21), but these requirements are relaxed for the more complicated structures.

The second contribution to the transmitted light is the thermal radiation from the slab, which is, of course, always present on both sides of the slab at nonzero temperatures. The spectrum of the thermal radiation generally shows oscillations related to the structure of the standing waves in the slab, but the oscillations are removed as the slab thickness is taken to infinity. The one-dimensional black-body spectrum is retrieved when the slab parameters are adjusted to ensure that all radiation falling on the slab is absorbed.

The formalism summarized in Sec. II, which embraces the same pulse propagation and reshaping phenomena as classical theory, is also capable of describing the effects of propagation through a dispersive and lossy slab on the nonclassical properties of an incident pulse, such as photon antibunching and squeezing. The topics will be pursued in a subsequent publication.

ACKNOWLEDGMENT

This work was supported by the European Community Human Capital and Mobility Programme through its network

on ''Nonclassical Light,'' with Contract No. CHRX-CT93-0114.

APPENDIX

In this appendix we evaluate the pulse contribution to the Poynting vector in Eq. (2.21) for the general case of an absorbing medium with $\kappa_c \neq 0$ and $2\omega_c \eta_c l/c \neq \pi n$. With the insertion of $T(\omega_c+\Omega)$ from Eq. (3.7) into Eq. (3.2) the relevant part of the integrand can be expressed as an exponential of the form

$$\exp\left\{ i\Omega\left[2l\left(k_c' - \frac{1}{c} + 2k_c' \frac{(n_c-1)^2}{D(\omega_c)} e^{4i\omega_c n_c l/c} \right) - t + \frac{x}{c} \right] \right\} \times \exp\left\{ -\Omega^2 \left[\frac{\mathcal{L}^2}{4c^2} + 8k_c'^2 l^2 \frac{(n_c^2-1)^2}{D^2(\omega_c)} e^{4i\omega_c n_c l/c} \right] \right\} \tag{A1}$$

with linear and quadratic terms in Ω having complex coefficients. The integration with respect to Ω is lengthy but it can be performed to obtain [18]

$$\langle :\hat{S}: \rangle_{pl} = S_0 \mathcal{I} \exp\left\{ - \frac{2\left[ct - x + 2l(1+F-E) - 64l \frac{l^2}{\mathcal{L}^2}(G+H)(AD+BC)/[1+32(l/\mathcal{L})^2(AC-BD)] \right]^2}{\mathcal{L}^2\left\{ 1 + 32\frac{l^2}{\mathcal{L}^2}(AC-BD) + \frac{l^4}{\mathcal{L}^4}[32(AD+BC)]^2/[1+32(l/\mathcal{L})^2(AC-BD)] \right\}} \right\}, \tag{A2}$$

where all the various constant prefactors omitted in Eq. (A1) are now gathered back together,

$$\mathcal{I} = \frac{\eta_c^2+\kappa_c^2}{(\Delta R)^2+(\Delta I)^2} \frac{\mathcal{L}^2}{l^2} \times \frac{e^{(G+H)^2/2[2(AC-BD)+(\mathcal{L}/4l)^2]}}{\{4(AD+BC)^2+[2(AC-BD)+(\mathcal{L}/4l)^2]^2\}^{1/2}} \tag{A3}$$

while S_0 is the incident peak power density defined in Eq. (3.5). The various parameters appearing in Eq. (A2) are

$$A = \frac{R_+R_- - I_+I_-}{(\Delta R)^2+(\Delta I)^2}; \quad B = \frac{R_+I_- + I_+R_-}{(\Delta R)^2+(\Delta I)^2}, \tag{A4}$$

$$C = c^2 \frac{[k_{cr}'\Delta R + k_{ci}'\Delta I]^2 - [k_{ci}'\Delta R - k_{cr}'\Delta I]^2}{(\Delta R)^2+(\Delta I)^2}, \tag{A5}$$

$$D = 2c^2 \frac{[k_{ci}'\Delta R - k_{cr}'\Delta I][k_{cr}'\Delta R + k_{ci}'\Delta I]^2}{(\Delta R)^2+(\Delta I)^2}, \tag{A6}$$

$$Ek_{ci}' = Hk_{cr}' = ck_{cr}'k_{ci}' \frac{(R_+^2-R_-^2)+(I_+^2-I_-^2)}{(\Delta R)^2+(\Delta I)^2} \tag{A7}$$

and

$$Fk_{cr}' = Gk_{ci}' = ck_{cr}'k_{ci}' \frac{\Delta R(I_++I_-) - \Delta I(R_++R_-)}{(\Delta R)^2+(\Delta I)^2}, \tag{A8}$$

where k_{cr}' and k_{ci}' are defined in Eq. (3.5). We set $\Delta R = R_+ - R_-$ and $\Delta I = I_+ - I_-$ with

$$\begin{aligned} R_+ &= (1-\kappa_+^2)(\eta_c+1)^2; \quad I_+ = 2\kappa_+(\eta_c+1)^2, \\ R_- &= (\eta_c-1)^2 e^{-4\omega_c\kappa_c l/c}\{(1-\kappa_-^2)\cos(4\omega_c\eta_c l/c) \\ &\quad - 2\kappa_-\sin(4\omega_c\kappa_c l/c)\}, \\ I_- &= (\eta_c-1)^2 e^{-4\omega_c\kappa_c l/c}\{2\kappa_-\cos(4\omega_c\eta_c l/c) \\ &\quad + (1-\kappa_-^2)\sin(4\omega_c\kappa_c l/c)\} \end{aligned} \tag{A9}$$

and $\kappa_\pm = \kappa_c/(\eta_c \pm 1)$.

[1] S. M. Barnett, R. Matloob, and R. Loudon, J. Mod. Opt. **42**, 1165 (1995).
[2] R. Matloob, R. Loudon, S. M. Barnett, and J. Jeffers, Phys. Rev. A **52**, 4823 (1995).
[3] C. G. B. Garrett and D. E. McCumber, Phys. Rev. A **1**, 305 (1970).
[4] S. Chu and S. Wong, Phys. Rev. Lett. **48**, 738 (1982).
[5] P. Halevi and R. Fuchs, Phys. Rev. Lett. **55**, 338 (1985).
[6] P. Halevi, Opt. Lett. **11**, 759 (1986).
[7] P. Halevi and J. A. Gaspar-Armenta, in *Surface Waves in Plasmas and Solids*, edited by S. Vukovic (World Scientific, Singapore, 1986), p. 147.
[8] P. Halevi and L. D. Valenzuela, J. Opt. Soc. Am. B **8**, 1512 (1991).
[9] J. A. Gaspar and P. Halevi, Phys. Rev. B **49**, 10 742 (1994).
[10] Y. Japha and G. Kurizki, Phys. Rev. A **53**, 586 (1996).
[11] T. Gruner and D.-G. Welsch, Acta Phys. Slovaca **46**, 387 (1996).
[12] A. M. Steinberg, P. G. Kwiat, and R. Y. Chiao, Phys. Rev. Lett. **71**, 708 (1993).
[13] Ch. Spielman, R. Szipöcs, A. Stingl, and F. Krausz, Phys. Rev. Lett. **73**, 2308 (1994).
[14] K. J. Blow, R. Loudon, S. J. D. Phoenix, and T. J. Shepherd, Phys. Rev. A **42**, 4102 (1990).

[15] C. K. Hong, Z. Y. Ou, and L. Mandel, Phys. Rev. Lett. **59**, 2044 (1987).
[16] M. S. Kim, L. Allen, and R. Loudon, Phys. Rev. A **50**, 3614 (1994).
[17] C. H. Monken and G. A. Barbosa, Opt. Commun. **99**, 152 (1993).
[18] E. S. Gradshteyn and I. M. Ryzhik, *Table of Integrals, Series, and Products* (Academic, New York, 1993).
[19] L. D. Landau, E. M. Lifshitz, and L. P. Pitaevskii, *Electrodynamics of Continuous Media* (Pergamon, Oxford, 1984).
[20] C. H. Henry and R. F. Kazarinov, Rev. Mod. Phys. **68**, 801 (1996).